Controllable Optical Phase Shift Over One Radian from a Single Isolated Atom

A. Jechow,* B. G. Norton, S. Händel, V. Blūms, E. W. Streed, and D. Kielpinski†

Centre for Quantum Dynamics, Griffith University, Brisbane 4111, Queensland, Australia

(Received 14 September 2012; published 14 March 2013)

Fundamental optics such as lenses and prisms work by applying phase shifts of several radians to incoming light, and rapid control of such phase shifts is crucial to telecommunications. However, large, controllable optical phase shifts have remained elusive for isolated quantum systems. We have used a single trapped atomic ion to induce and measure a large optical phase shift of 1.3 ± 0.1 radians in light scattered by the atom. Spatial interferometry between the scattered light and unscattered illumination light enables us to isolate the phase shift in the scattered component. The phase shift achieves the maximum value allowed by atomic theory over the accessible range of laser frequencies, pointing out new opportunities in microscopy and nanophotonics. Single-atom phase shifts of this magnitude open up new quantum information protocols, in particular long-range quantum phase-shift-keying cryptography.

DOI: 10.1103/PhysRevLett.110.113605 PACS numbers: 42.50.Ct, 32.10.−f, 37.10.Ty, 42.50.Gy

Optical phase shifts are commonly observed from all materials, and generally originate from the delayed response of electrons to an applied light field. All refractive optics, including such fundamental optics such as lenses and prisms, work by applying spatially varying phase shifts of several radians to incoming light. In fiber-optical telecommunications systems, rapid control of phase shifts allows encoding of information in the widely used phase-shift-keying protocol [1]. In principle, strong phase shifts persist down to the single-atom level. As the frequency of light is tuned around atomic resonance, semiclassical theory predicts that the scattered light experiences a phase advance of 0 for far red detuning, through $\pi/2$ on resonance, to π for far blue detuning.

However, large, controllable optical phase shifts have remained elusive for isolated quantum systems. Weak phase shifts have recently been observed from single atoms [2] and molecules [3]. Similar small phase shifts, arising from the shift of atomic energy levels, have also been observed by interferometric measurements of fluorescence from single trapped ions [4]. The interferometric techniques used in those experiments analyzed only the on-axis interference between the scattered field and the illumination field, so the properties of the scattered field could not be studied in isolation. Since the illumination field is always much stronger than the scattered field in these configurations, the accessible phase shift was limited at the 100 mrad level by the scattering amplitude, restricting applications in quantum information processing and nanophotonics. In another approach, by confining an atom in a high-finesse optical cavity, the phase shift effect was magnified by recycling the illumination light through the atom [5]. Superconducting qubits in 1D transmission lines have also been observed to impart radian-level phase shifts to the guided microwave radiation [6]. The Wigner scattering delay for a single atom, which is related to the frequency derivative of the phase shift at resonance, has also been measured contemporaneously with the present work [7].

Here we demonstrate access to controllable radian-level phase shifts of scattered light for an isolated atomic ion in free space and without the need for a cavity. For the first time to our knowledge, the scattering phase for a single atom is demonstrated to achieve its theoretical limit. Laser-cooled, trapped atomic ions are nearly ideal systems for investigating quantum optics: they can remain trapped for hours and are nearly perfectly isolated from their environment [8]. Our experimental apparatus is similar to that used in our recent work [9,10]. A schematic of the apparatus is shown in Fig. 1. A single $^{174}Yb^{+}$ ion is trapped in ultrahigh vacuum using a double-needle radio-frequency (rf) quadrupole Paul trap operating at a drive frequency of 40 MHz. Laser light at 369.5 nm, near resonance with a strong transition of the ion, is weakly focused onto the ion to provide an illumination field with power of ~5 nW and spot diameter of 5 μm (full-width at half-maximum). The illumination beam is linearly polarized to eliminate optical pumping effects and its power is actively stabilized to minimize intensity fluctuations between reference and signal images. The light transmitted past the atom is reimaged onto a cooled CCD camera with a magnification of 585. To provide additional laser cooling, an auxiliary 369.5 nm laser beam, detuned −200 MHz from atomic resonance, is applied perpendicular to the optical axis. This additional cooling enables us to tune the illumination field somewhat blue of resonance while maintaining reasonable image contrast. The laser cooling ensures that the amplitude of the ion's motion stays at or below the imaging resolution, even at blue detuning. All data presented here have been obtained from a single continuously trapped ion over a period of a few hours.

Our data consist of background-subtracted, normalized images of the light transmitted past a single trapped ion, which amount to spatial interferograms of the light field

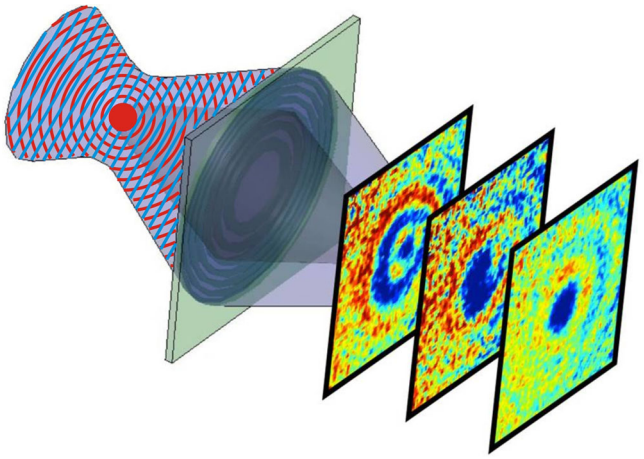

FIG. 1 (color online). Configuration of experimental apparatus. A laser cooled $^{174}Yb^{+}$ ion (red dot) is confined in a radio-frequency electric quadrupole trap generated by two tungsten needles. Resonant laser light at $\lambda = 369.5$ nm is incident along the optical axis of the imaging system (the left side of the figure) and weakly focused at the ion position, illuminating the ion with a plane wave. The transmitted light consists of a superposition of the scattering and driving field, with phase fronts depicted by lines in the vicinity of the ion. The transmitted light is imaged with a large aperture phase Fresnel lens [9,11] and a weak refocusing lens (not shown) onto a cooled CCD camera at 585 × magnification. We acquire images of the transmitted light at several camera viewing planes. A secondary cooling beam (not shown) is incident orthogonal to the needle axis and the optical axis.

scattered by the ion. These images are obtained by subtracting signal images, for which ion absorption was present, from reference images of the illuminating beam. Each pixel of the subtracted image is then normalized to its value in the reference image. To acquire the reference images, we optically pump the ion into the metastable $D_{3/2}$ atomic state, which scatters only a negligible amount of the 369.5 nm light. In the observation plane (i.e., the plane imaged onto the camera), the intensity of the scattered field $U_{sc}(x, y)$ is everywhere much smaller than the intensity of the illumination field $U_0(x, y)$. Within the image area, the illumination field intensity is nearly uniform and is independent of the observation plane position, so the phase and amplitude of the illumination field is nearly uniform. Our illumination method is therefore entirely distinct from recent experiments [2,3] that used tightly focused (wavelength-scale) laser beams and single-mode detection to probe scattering properties of isolated atoms and molecules. The background-subtracted, normalized image signal, denoted $S(x, y)$, is given by

$$S(x, y) \propto |U_0(x, y) + U_{sc}(x, y)|^2 - |U_0(x, y)|^2 \approx 2\,\mathrm{Re}[U_{sc}(x, y)U_0(x, y)] \propto \mathrm{Re}[U_{sc}(x, y)], \quad (1)$$

where the third line follows from the fact that $U_0(x, y)$ is approximately constant. The vector character of the electric field is neglected, as is appropriate at our numerical aperture of 0.64. The image signal $S(x, y)$ is seen to be a spatial interferogram of the scattered field, with the illumination field serving as the reference wave. Unlike our recent work on absorption imaging, which investigated the removal of light from the illumination mode [10], here we exploit constructive and destructive interference patterns to retrieve the scattering phase.

The high information content of the spatial interferogram $S(x, y)$ enables us to isolate the parameters of the scattered field $U(x, y)$, in particular the phase shift. The total transmitted field amplitude $U_0(x, y) + U_{sc}(x, y)$ exhibits only small phase shifts relative to the illumination field in our data. Nevertheless, in order to match the spatial dependence of $S(x, y)$ to well-understood models of wave optics, we are constrained to assign large phase shifts to the scattered component of the total field. The imaging technique therefore accesses the scattered field alone, in contrast to results from previous measurements that recorded interference effects in a single optical mode [2,3]. Since those previous measurements only probed the total transmitted power, the large-amplitude illumination field overwhelmed the small-amplitude scattered wave contribution. Hence, the phase shift observed in those measurements was always reduced by a factor of $U_{sc}/U_0 < 0.1$ relative to the results presented here, accounting for the previous observations of $\lesssim 100$ mrad phase shifts.

Figure 2 shows a series of single-ion interferograms at different observation planes and laser detunings. When

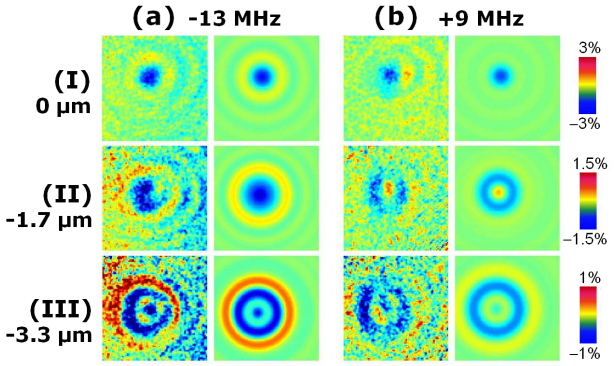

FIG. 2 (color online). Spatial interferograms of the scattered wave. The theoretical prediction for each interferogram is shown to the right of the data. The image resolution is 370 nm, approximately equal to the illumination wavelength of 369.5 nm, and each image is 3.4 μm on a side. Each row of images corresponds to a fixed observation plane position. In terms of the object space coordinates, row I sits at the nominal plane of the ion and row II (respectively, III) at 1.7 μm (respectively, 3.3 μm) upstream of the ion. The color bars at the right of the figure indicate the fractional change in transmission for the images in each row. The images are smoothed with a Gaussian filter of 40 nm width for ease of viewing, but only raw data are used for comparison with theory. (a) Data (left) and theory (right) at −13 MHz detuning. (b) The same, but for +9 MHz detuning.

the imaging system is focused at the plane of the ion (row I in Fig. 2), the scattered light always interferes destructively with the transmitted light, giving rise to an absorption image of the ion. The contrast of the absorption image, as well as the detuning dependence of the contrast, accords with the semiclassical theory of the atom-light interaction and with our previous measurements [10]. For defocused imaging (rows II and III in Fig. 2), the interference of the approximately spherical scattered wave with the planar illumination wave gives rise to a "bullseye" pattern. The extent of the bullseye grows with increasing defocusing as the scattered wave spreads transversely. The detuning-dependent phase shift of the scattered wave induces an alteration of the interference pattern, which is immediately evident from the on-axis intensity in row II and more subtly affects the spacing of the interference rings in row III. Slight nonuniformities in the illumination beam intensity, combined with small drifts of the pointing, cause significant shot-to-shot variations in the background-subtracted data images of Fig. 2. These variations can give rise to spurious apparent structures in the images. Nevertheless, the overall agreement with the model remains clear.

Despite the presence of the auxiliary red-detuned cooling beam, we still incur reduced image contrast when the illumination beam is blue-detuned, but the reduced contrast does not affect our ability to measure the phase shift. The auxiliary cooling beam intensity is kept relatively low to avoid excessive saturation of the atomic transition, so the ion temperature still rises above the Doppler limit for blue detuning. The resulting thermal motion reduces the effective imaging resolution at blue detuning [12]. Along with residual saturation by the auxiliary beam, the lower resolution accounts for the difference in contrast between Figs. 2(a) and 2(b). The cooling beam also imparts an ac Stark shift to the atomic levels, which is calculated to be negligible for our experiment.

We determine the phase of the scattered wave at each detuning from a series of interferogram images similar to those shown in Fig. 2. For each image series, the detuning is fixed and the observation plane is shifted to several positions along the optic axis. Each image series is fitted to a simulation of the wave propagation through our imaging system, and the scattered wave parameters are extracted from the fit. Typical fit images are shown in Fig. 2.

Our simulations use scalar diffraction theory to model optical propagation through our imaging system. In particular, the scattered wave is taken to be a scalar spherical wave. This assumption is well justified for our numerical aperture (NA) of 0.64, since our geometry restricts the scattered polarization to $\sigma^{\pm}$ along the imaging axis [13]. The illumination field is modeled as a low-NA Gaussian beam with standard Gaussian beam propagation theory. The spherical scattered wave is propagated nonparaxially up to the Fresnel lens and then propagated through the (weak) refocusing lens to the image plane using the Fresnel approximation. When used to simulate fluorescence images, this model leads to good agreement with experimental data previously collected with our apparatus [9].

We model the Fresnel lens as a near-perfect lens with a small amount of spherical aberration and a super-Gaussian pupil function. The Fresnel lens is modeled as a thin complex transmittance. The transmittance phase removes nearly all of the off-axis spatial phase variation of the scattered spherical wave, leaving only the spherical aberration phase function $\Phi(\rho) = A\rho^4$, where ρ is the distance from the optic axis in the plane of the Fresnel lens and A quantifies the magnitude of spherical aberration. The transmittance amplitude is taken to be a super-Gaussian function $p_S \propto e^{-\rho^4/\rho_0^4}$, defining the diffraction-limited resolution of the imaging system through the pupil parameter ρ_0.

When the imaging system is close to being in focus, the scattered field in the image plane (x, y) is found to be

$$U_{\mathrm{sc}}(\xi) = -U_0 a_{\mathrm{sc}} e^{i\phi_{\mathrm{sc}}} \frac{i e^{-ik(f_F+f_R)}}{\lambda f_R} \tilde{u}_{\mathrm{sc}}\left(\frac{\xi}{\lambda f_R}\right), \quad (2)$$

$$\tilde{u}_{\mathrm{sc}} \equiv \mathcal{F}\left[\exp[i\pi\zeta\rho^2/(f_F^2\lambda)] \frac{p_S(\rho)}{\sqrt{f_F^2+\rho^2}}\right], \quad (3)$$

for small deviations of the viewing plane ζ along the optic axis, measured relative to the in-focus image plane. Here $\xi = \sqrt{x^2+y^2}$ is the transverse distance from the optic axis in the image-plane coordinates, the drive field amplitude is U_0, the atomic scattering amplitude and phase are a_{sc} and ϕ_{sc}, the Fresnel lens focal length is f_F, the reimaging lens focal length is f_R, and $\mathcal{F}[g]$ denotes the two-dimensional Fourier transform of a function $g(x, y)$. The fit function for our image data is the real part of Eq. (2), following the discussion in the text around Eq. (1).

The retrieved phase of the scattered wave is shown as a function of detuning in Fig. 3(a). The close agreement with atomic theory, observed here for the first time to our knowledge, evidences the near-ideal character of our system. Since the intensity of the illumination is kept well below the saturation intensity of the atomic transition (600 W cm^{-2}), the semiclassical theory of atomic scattering in a weak laser field should apply. In our case, this theory is equivalent to treating the atomic dipole as a damped simple harmonic oscillator driven by the laser field. The phase ϕ then depends only on the laser detuning Δ as follows:

$$\phi(\Delta) = \tan^{-1}(\Delta/\Gamma) + \pi/2, \quad (4)$$

where Γ is the atomic linewidth (full-width at half maximum). The scattering probability, shown for comparison in Fig. 3(b), is proportional to $1/[\Delta^2 + (\Gamma/2)^2]$. On the blue side of atomic resonance, ion heating causes Doppler broadening of the linewidth above the nominal linewidth of 20 MHz exhibited by an ideal $^{174}Yb^+$ ion at rest. This effect, which is common to all trapped-ion experiments,

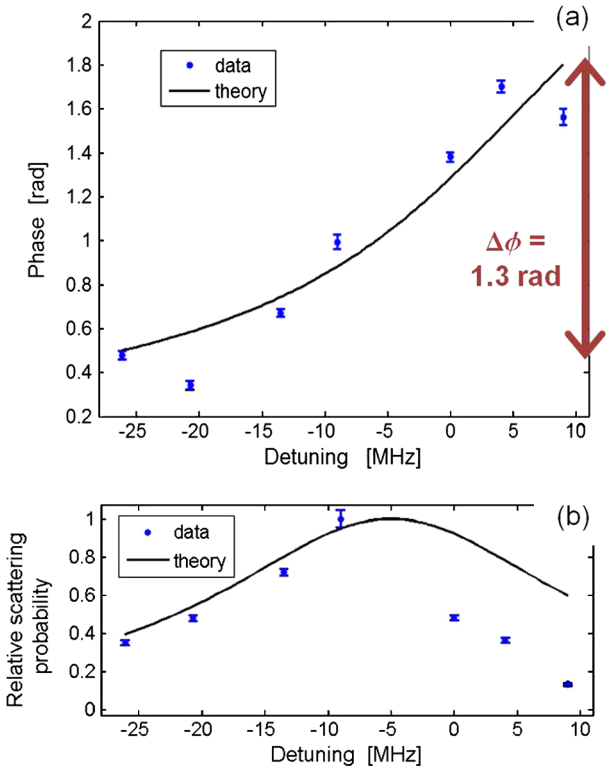

FIG. 3 (color online). Phase shift and normalized scattering probability of the scattered wave. (a) Phase of the scattered wave as a function of laser detuning. Each data point is obtained by fitting a series of spatial interferograms to the model. The data show a total phase shift of 1.3 ± 0.1 radians. The uncertainty in determining spherical aberration imparts a common systematic error of ± 0.1 rad to all data points. This common-mode error does not affect the measurement of the phase shift. The data is well fit by semiclassical theory with the linewidth $\Gamma = 34 \pm 8$ MHz, with the fitted resonance position shifted 5 ± 2 MHz blue of the nominal resonance frequency. (b) Normalized scattering probability as a function of detuning. All values are normalized to the maximum scattering probability observed in the data. The theory curve is predicted from the fit to the phase shift. On resonance and at blue detuning, the scattering probability is lower than expected from the theory. The mechanical effects of the laser light are seen to be significant, including the broadening and redshift of the phase-shift data relative to the ideal case.

broadens the scattering phase feature and lowers the scattering probability at blue detuning. Similarly, our fluorescence measurement of the resonance frequency is expected to underestimate the actual frequency, since ion heating lowers the fluorescence rate rapidly to the blue of resonance. We fit the phase measurements to the semiclassical model of Eq. (4) and find $\Gamma = 34 \pm 8$ MHz, with the fitted resonance position shifted 5 ± 2 MHz blue of the nominal resonance frequency. The fit values from the phase function are then used to obtain a prediction for the scattering probability in Fig. 3(b). The predicted scattering probability agrees well with the data (except when ion heating is known to be significant), confirming the validity of our phase measurements.

Our observation of single-atom phase shifts at the theoretical limit holds wide implications for microscopy and nanophotonics. Our results verify that the large optical phase shifts predicted by quantum theory can actually be observed in practice, calibrating the capabilities of techniques based on phase shifts. For instance, x-ray phase contrast microscopy is a powerful technique for medical imaging [14] in which low light levels are crucial to avoid side effects: our results verify that the contrast of low-light phase images can achieve its theoretical limit. Similarly, nanoplasmonic device engineering is now pushing toward few-atom phase modulators [15], in which the controllable phase shift per atom gives a fundamental limit to device performance.

Our results also point to new protocols in quantum communication. Quantum phase-shift-keying (QPSK) cryptography with single photons [16] has already been demonstrated to be extremely resistant to decoherence and channel loss [17]. A single-atom phase shifter can serve as a quantum repeater node for QPSK, so that entanglement-swapping protocols can enable QPSK cryptography over long distances. Our present experimental system, in which the 369.5 nm transition of $^{174}Yb^{+}$ is illuminated by π-polarized light, is ideal for this purpose. Application of a magnetic field imposes Zeeman splitting on both the ground and excited states, so that the π transition is split into two components corresponding to the two ground-state Zeeman levels $|\downarrow\rangle$, $|\uparrow\rangle$. Suppose that the magnetic field is large and the illumination frequency is tuned halfway between the Zeeman-split transition frequencies. Then a single scattered photon will experience a phase shift of 0 if the atom is in $|\downarrow\rangle$ and π if the atom is in $|\uparrow\rangle$, generating the entangled atom-photon state $|\downarrow\rangle|0\rangle + |\uparrow\rangle|\pi\rangle$. If we detect quantum interference between the photons emitted by two atomic nodes, the atoms will be projected into an entangled state, establishing a quantum repeater link [18]. In a similar scenario, one could imagine generation of multiphoton states whose phase shift is entangled with the internal state of an ion. Such multiphoton states could conceivably improve the accuracy of atomic state detection.

This work was supported by the Australian Research Council under FT110100513 (D. K., Future Fellowship) and DP0877936 (E. W. S., Australian Postdoctoral Fellowship). A. J. was also supported by a Griffith University Postdoctoral Fellowship. The phase Fresnel lens was fabricated by M. Ferstl at the Heinrich-Hertz-Institut of the Fraunhofer-Institut für Nachrichtentechnik in Germany.

*Present address: Institute of Physics and Astronomy, Photonics, University of Potsdam, 14476 Potsdam-Golm, Germany.
†d.kielpinski@griffith.edu.au

[1] A. Gnauck and P. Winzer, J. Lightwave Technol. **23**, 115 (2005).
[2] S. A. Aljunid, M. K. Tey, B. Chng, T. Liew, G. Maslennikov, V. Scarani, and C. Kurtsiefer, Phys. Rev. Lett. **103**, 153601 (2009).
[3] M. Pototschnig, Y. Chassagneux, J. Hwang, G. Zumofen, A. Renn, and V. Sandoghdar, Phys. Rev. Lett. **107**, 063001 (2011).
[4] M. A. Wilson, P. Bushev, J. Eschner, F. Schmidt-Kaler, C. Becher, R. Blatt, and U. Dorner, Phys. Rev. Lett. **91**, 213602 (2003).
[5] J. Kerckhoff, M. A. Armen, D. S. Pavlichin, and H. Mabuchi, Opt. Express **19**, 6478 (2011).
[6] O. Astafiev, A. Zagoskin, A. Abdumalikov, Jr., Y. Pashkin, T. Yamamoto, K. Inomata, Y. Nakamura, and J. Tsai, Science **327**, 840 (2010).
[7] R. Bourgain, J. Pellegrino, Y. Sortais, and A. Browaeys, arXiv:1210.0389.
[8] D. Leibfried, R. Blatt, C. Monroe, and D. Wineland, Rev. Mod. Phys. **75**, 281 (2003).
[9] A. Jechow, E. Streed, B. Norton, M. Petrasiunas, and D. Kielpinski, Opt. Lett. **36**, 1371 (2011).
[10] E. W. Streed, A. Jechow, B. G. Norton, and D. Kielpinski, Nat. Commun. **3**, 933 (2012).
[11] E. W. Streed, B. G. Norton, A. Jechow, T. J. Weinhold, and D. Kielpinski, Phys. Rev. Lett. **106**, 010502 (2011).
[12] B. G. Norton, E. W. Streed, M. J. Petrasiunas, A. Jechow, and D. Kielpinski, New J. Phys. **13**, 113022 (2011).
[13] E. W. Streed, B. G. Norton, J. J. Chapman, and D. Kielpinski, Quantum Inf. Comput. **9**, 0203 (2009).
[14] F. Arfelli *et al.*, Phys. Med. Biol. **43**, 2845 (1998).
[15] D. K. Gramotnev and S. I. Bozhevolnyi, Nat. Photonics **4**, 83 (2010).
[16] K. Inoue, E. Waks, and Y. Yamamoto, Phys. Rev. Lett. **89**, 037902 (2002).
[17] H. Takesue, S. W. Nam, Q. Zhang, R. H. Hadfield, T. Honjo, K. Tamaki, and Y. Yamamoto, Nat. Photonics **1**, 343 (2007).
[18] L.-M. Duan, M. D. Lukin, J. I. Cirac, and P. Zoller, Nature (London) **414**, 413 (2001).